

Journal of Materials Chemistry B

Accepted Manuscript



This is an *Accepted Manuscript*, which has been through the Royal Society of Chemistry peer review process and has been accepted for publication.

Accepted Manuscripts are published online shortly after acceptance, before technical editing, formatting and proof reading. Using this free service, authors can make their results available to the community, in citable form, before we publish the edited article. We will replace this *Accepted Manuscript* with the edited and formatted *Advance Article* as soon as it is available.

You can find more information about *Accepted Manuscripts* in the [Information for Authors](#).

Please note that technical editing may introduce minor changes to the text and/or graphics, which may alter content. The journal's standard [Terms & Conditions](#) and the [Ethical guidelines](#) still apply. In no event shall the Royal Society of Chemistry be held responsible for any errors or omissions in this *Accepted Manuscript* or any consequences arising from the use of any information it contains.

One-pot synthesis of CuFe_2O_4 magnetic nanocrystal clusters for highly specific separation of histidine-rich proteins

Cite this: DOI: 10.1039/x0xx00000x

Received 00th January 2012,
Accepted 00th January 2012

DOI: 10.1039/x0xx00000x

www.rsc.org/

Jiangnan Zheng, Zian Lin,* Wei Liu, Ling Wang, Sen Zhao, Huanghao Yang, and Lan Zhang**

This work reports a facile ligand-free method for the rapid and highly specific separation of histidine (His)-rich proteins by using CuFe_2O_4 magnetic nanocrystal clusters (MNCs). Monodisperse CuFe_2O_4 MNCs were synthesized *via* a simple and economical one-pot hydrothermal process. The resulting MNCs were characterized in detail. The measurements indicated that the MNCs exhibited good dispersion, high crystallinity, and superparamagnetic properties. Moreover, the obtained MNCs had a high saturation magnetization (45.1 emu g^{-1}), which was sufficient to accomplish fast and efficient separation with an external magnetic field. The selectivity and binding capacity of CuFe_2O_4 MNCs were evaluated by using a His-rich protein (bovine haemoglobin) and other proteins (bovine serum albumin, human serum albumin, myoglobin, lysozyme, cytochrome c and horseradish peroxidase) containing less surface-exposed His residues as model samples. The most distinct feature of the CuFe_2O_4 MNCs is the high haemoglobin binding capacity (4475 mg g^{-1}) owing to the coordination between Copper (II) ions and surface-exposed histidine residues of haemoglobin. In addition, the CuFe_2O_4 MNCs can be successfully employed to selectively bind and removal abundant protein haemoglobin from human blood samples. The good results demonstrated their potential in separation of His-rich proteins.

Introduction

Histidine (His)-rich proteins are characteristic biomolecules that play crucial roles in various physiological processes.¹ For example, prion proteins (PrPs) are extremely His-rich and crucial for the prion pathogenesis. Another well studied example is *Plasmodium falciparum* His-rich protein II, which has been recognized as a malarial biomarker.² Therefore, the isolation of His-rich proteins from biological samples is essential for ongoing proteomics, and for therapeutic and diagnostic applications. Among the techniques used for this, immobilized metal affinity chromatography (IMAC) is the most widely used method. However, it is unsuitable for complex biological samples containing suspended solids and fouling components. Therefore, establishment of novel methods for highly selective separation of His-rich proteins is necessary. These methods should be capable of treating biological samples with a wide range of protein concentrations in large-scale processes, even in the presence of particulate mixtures.

Magnetic nanoparticles (MNPs) have gained considerable attention in proteomics and peptidomics analysis due to their magnetism properties, uniform morphology, and ease of surface modification.³ Protein separation by functionalized MNPs is usually based on the surface modification of affinity ligands.⁴

MNPs with IMAC has been used to selectively separate His-tagged recombinant proteins or natural His-rich proteins from complex samples.⁵⁻¹⁵ For example, Xu and co-workers used dopamine as a stable anchor to attach nitrilotriacetic acid (NTA) ligands on the surface of MNPs, and the resulting products reacted with NiCl_2 to obtain $\text{MNP-DA-NTA-Ni}^{2+}$ for selective binding to His-tagged proteins.^{5,6} Chen and co-workers reported a series of methods to synthesize iminodiacetic acid (IDA) immobilized MNPs, and then charged with Cu^{2+} or Ni^{2+} for selective capture of His-rich bovine hemoglobin (BHb).⁹⁻¹³ Nevertheless, these MNPs with IMAC methods usually need several steps to conjugate proper ligands on the MNPs. Moreover, these ligands are either expensive or inconvenient to obtain. In order to design a simpler and more efficient method for the separation of His-tagged proteins, functional MNPs based on metal oxide affinity chromatography (MOAC) were developed.¹⁶⁻²⁰ For instance, Hyeon and co-workers synthesized Ni/NiO core-shell MNPs to efficiently purify His-tagged proteins from the mixed protein solution.¹⁴ On the same principle, nickel-doped magnetite, NiO-decorated MNPs, and nickel silicate-coated magnetic heterostructures have also been developed.¹⁷⁻²⁰ These systems, however, still suffer from drawbacks such as low magnetic response,

complicated synthesis routes, and severe aggregation of nanomaterials. In addition, all these reports focused on the separation of His-tagged proteins, but the isolation of natural His-rich proteins using MNPs-based MOAC has not been well documented.

As one of transition metal ferrites, CuFe_2O_4 material has been studied in the fields of electronics²¹ and catalysis²². Very recently, hierarchically porous CuFe_2O_4 nanospheres were reported as excellent electrode material in supercapacitor.²³ However, the protein- CuFe_2O_4 interaction has not been investigated till now as far as we know.

In this study, we first reported a ligand-free strategy for the selective capturing natural His-rich proteins by using CuFe_2O_4 magnetic nanocrystal clusters (MNCs). The properties of CuFe_2O_4 MNCs synthesized by a simple one-pot hydrothermal route were characterized in detail. The affinity of the CuFe_2O_4 MNCs toward several natural proteins which containing different numbers of surface-exposed His residues were examined. In addition, the practicability for biological application was further assessed by isolation and depletion of hemoglobin from human whole blood.

Experimental

Materials

Ferric chloride hexahydrate ($\text{FeCl}_3 \cdot 6\text{H}_2\text{O}$), Copper (II) chloride ($\text{CuCl}_2 \cdot 2\text{H}_2\text{O}$), sodium acetate (NaAc), ethylene glycol, and trisodium citrate dihydrate ($\text{Na}_3\text{Cit} \cdot 2\text{H}_2\text{O}$) were obtained from Sinopharm Chemical Reagent, Co., Ltd. (Shanghai, China). Sequencing-grade modified trypsin (TPCK-trypsin), L-histidine (99%) and trifluoroacetic acid (TFA) were obtained from Aladdin Chemistry Co., Ltd (Shanghai, China). BHB, bovine serum albumin (BSA) and horseradish peroxidase (HRP) were purchased from Shanghai Lanji Co. Ltd. (Shanghai, China). Myoglobin from equine skeletal muscle (Mb, M1882), lysozyme from chicken egg white (Lyz, L7651) and cytochrome c from equine heart (Cyt C, Sigma C2867) were the products of Sigma-Aldrich (St. Louis, MO, USA). Healthy human blood was kindly donated by Fujian Provincial Official Hospital (Fuzhou, China). Deionized water ($18.2 \text{ M}\Omega \text{ cm}^{-1}$) was prepared with a Milli-Q water purification system (Millipore, USA). All reagents above were of analytical grade or better.

Preparation of CuFe_2O_4 MNCs

The CuFe_2O_4 MNCs were prepared by a solvothermal reaction at 200°C . Briefly, $\text{FeCl}_3 \cdot 6\text{H}_2\text{O}$ (4.050 g, 15 mmol), $\text{CuCl}_2 \cdot 2\text{H}_2\text{O}$ (1.278 g, 7.5 mmol), NaAc (8.2 g, 100 mmol), $\text{Na}_3\text{Cit} \cdot 2\text{H}_2\text{O}$ (29.4 mg, 0.1 mmol) were dissolved in ethylene glycol (100 mL). The obtained homogeneous solution was transferred to autoclave, and then heated to 200°C for 12h. After reaction, the product was rinsed with water and ethanol for several times and dried at room temperature.

In-vial adsorption and separation of proteins

The isothermal binding and kinetic adsorption tests were performed in the same way as described in our previous work.^{24,25} All sample solutions were prepared in 20 mM phosphate buffer solution (PBS) containing 0.2 M NaCl (pH 7.0). In the isothermal adsorption experiments, 0.050 mg of CuFe_2O_4 MNCs were vortex-mixed with 1 mL of BHB solution at different concentrations ranged from 0.10 to 1.0 mg mL^{-1} for 10 min in the centrifuge tube at room temperature. Then, the MNCs-proteins conjugates were isolated by placing an external magnet on the wall of the tube. After magnetic separation, the supernatants were collected and the protein concentrations of the supernatants were individually determined by HPLC. The equilibrium adsorption capacity (Q_e , mg g^{-1}) was calculated according to the following formula (Equation 1):

$$Q_e = \frac{(C_0 - C_e)V}{m} \quad (1)$$

where C_0 is the initial protein concentration (mg mL^{-1}), C_e is the supernatant protein concentration (mg mL^{-1}), V is the volume of protein solution (mL) and m is the weight of the MNCs (g). The adsorption isotherms were fitted by the Langmuir model (Equation 2),

$$\frac{C_e}{Q_e} = \frac{1}{bQ_m} + \frac{1}{Q_m} C_e \quad (2)$$

where b is the Langmuir constant that directly relates to the adsorption affinity (L mg^{-1}), Q_m is the saturated capacity (mg g^{-1}), respectively. Q_m and b can be calculated by plotting C_e/Q_e as a function of C_e .

In the kinetic binding experiments, 0.050 mg of CuFe_2O_4 MNCs were incubated with 1 mL of BHB solution for different incubation times ranged from 0 to 60 min at room temperature. The adsorption capacity (Q_t) was quantified as mentioned above. To investigate the kinetic mechanisms of binding, the adsorption kinetics was fitted by the pseudo-second-order kinetic model (Equation 3)

$$\frac{t}{Q_t} = \frac{1}{k_2 Q_e^2} + \frac{t}{Q_e} = \frac{1}{V_0} + \frac{t}{Q_e} \quad (3)$$

where Q_t is the adsorption capacity (mg g^{-1}) after shaking a time of t (min), k_2 is the rate constant ($\text{g mg}^{-1} \text{min}^{-1}$), and V_0 is the initial adsorption rate ($\text{mg g}^{-1} \text{min}^{-1}$), respectively.

In the selective adsorption experiments, 0.40 mg of CuFe_2O_4 or Fe_3O_4 MNCs was incubated with 1 mL of a mixed solution of 0.40 mg mL^{-1} BSA and 1.20 mg mL^{-1} BHB in binding buffer for 10 min. After magnetic separation, the supernatants were collected. Then the MNCs-proteins conjugates were rinsed with binding buffer for several times. The captured species were eluted with 10 mM His solution containing 0.2 M NaCl. The supernatants and the eluates were analyzed by HPLC.

Reusability of CuFe_2O_4 MNCs

To estimate the reusability of CuFe_2O_4 MNCs, 0.2 mg of MNCs was incubated with 0.5 mL of BHb at a concentration of 0.80 mg mL^{-1} for 10 min at room temperature. After magnetic separation, the supernatants were collected. The MNCs-protein conjugates were washed by 100 mM Na_2CO_3 - NaHCO_3 buffer (pH10) and deionized water several times, then reused for the adsorption of BHb.

Real sample analysis

The CuFe_2O_4 MNCs were applied to specifically separate human hemoglobin (HHb) from a real sample of bovine blood. The sample was diluted 100-fold with binding buffer and incubated with CuFe_2O_4 MNCs for 10 min at room temperature, and then the captured species were eluted with 10 mM His solution containing 1% SDS. The diluted blood sample, supernatant, and eluent were collected and analyzed by sodium dodecyl sulfate polyacrylamide gel electrophoresis (SDS-PAGE). The loading amount of sample is 10 μL .

Characterization

Scanning electron microscopy (SEM) images were obtained with FEI Inspect F50 (FEI, USA). Transmission electron microscopy (TEM) analyses were performed on a FEI Tecnai G2 20 (FEI, USA) at 200 kV. The Brunauer-Emmett-Teller (BET) specific surface areas of typical products were measured using an ASAP 2020 (Micromeritics, USA). Fourier-transform infrared (FT-IR) spectra were taken on Nicolet 6700 spectrometer (Thermo Fisher, USA) using KBr pellets. The X-ray powder diffraction (XRD) pattern was determined by X'Pert-Pro MPD (Philips, Holland). The magnetization curves were carried out at room temperature on the LDJ 9600 (LDJ Electronics, Troy, MI) vibrating sample magnetometer (VSM). All chromatographic measurements were performed by Shimadzu Prominence LC-20A series HPLC (Kyoto, Japan) and an Agela Technologies Venusil XBP C8 (100 mm \times 4.6 mm, 5 μm , 300 \AA) column (Tianjin, China). The proteins were eluted with a linear gradient from 5% to 80% buffer B (buffer A, 0.1% TFA in water; buffer B, 0.07% TFA in ACN) over 5 min at a flow rate of 1.5 mL/min at 40 $^\circ\text{C}$. The injected sample volume was 20 μL , and the samples were detected using the UV detector (280 nm for BSA, HSA, Lyz; 406 nm for BHb, Mb, Cyt C and HRP). Quantitative analysis of the protein solutions were performed from a linear calibration curve of peak area versus concentration. Electrophoresis of proteins was performed using regular SDS-PAGE (Bio-Rad, CA, USA) with 10% running and 5% stacking gels. Proteins were stained with Coomassie Brilliant Blue R-250.

Results and discussion

Preparation and characterization of CuFe_2O_4 MNCs.

The citrate-stabilized MNCs were prepared using a simple solvothermal route by reaction of $\text{FeCl}_3 \cdot 6\text{H}_2\text{O}$, $\text{CuCl}_2 \cdot 2\text{H}_2\text{O}$ and ethylene glycol in the presence of NaAc as an alkali source and Na_3Cit as an electrostatic stabilizer (Fig. 1). The formation

of MNCs follows the well-documented two-stage growth model in which primary nanocrystals nucleate first in a supersaturated solution and then aggregate into larger secondary particles.^{26,27}

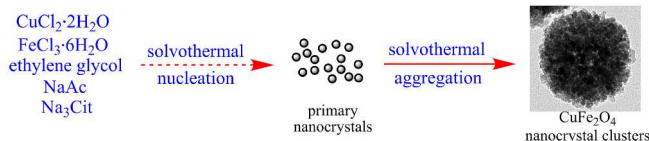


Fig. 1 Schematic representation of the two-stage growth mechanism of the CuFe_2O_4 MNCs

The morphology and structure of the resulting product were investigated by using SEM and TEM. Representative SEM and TEM images showed that the synthesized CuFe_2O_4 MNCs were nearly spherical in shape and had an average diameter of 170 nm (Fig. 2A and B). The secondary structure of MNCs can be observed more clearly in TEM image at higher magnification. The MNCs are composed of nanocrystals with a size of about 6–15 nm (Fig. 2C). Further details concerning these nanocrystals are obtained by the high-resolution TEM (HRTEM). As shown in the HRTEM image and corresponding fast Fourier Transform (FFT) pattern of MNCs (Fig. 2D), the distances between two adjacent planes in two different direction were measured as 0.30 nm and 0.25 nm, which correspond well to the lattice spacing of (220) and (311) planes of fcc CuFe_2O_4 .

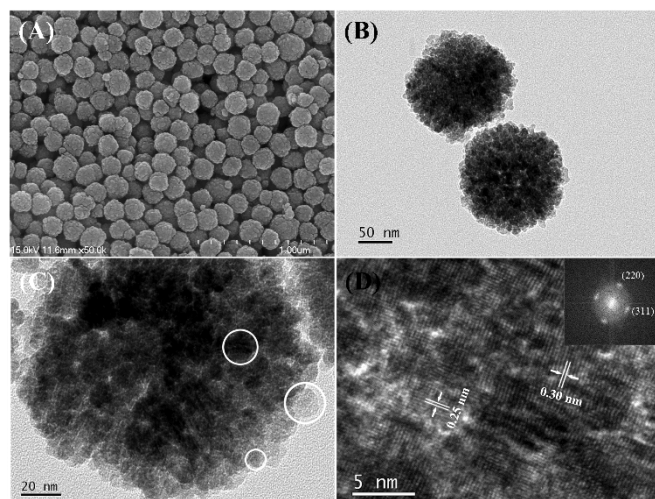


Fig. 2 SEM (A) and TEM (B) images of CuFe_2O_4 MNCs. (C) TEM image at higher magnification. (D) Lattice-resolved HRTEM image of CuFe_2O_4 MNCs and corresponding FFT pattern (top-right inset).

The composition of the resulting MNCs was observed by energy dispersive X-ray spectrometry (EDS). As shown in Fig. S1†, Cu, Fe, and O were the three main elements found, indicating that it was possible for well-structured CuFe_2O_4 materials to be obtained.

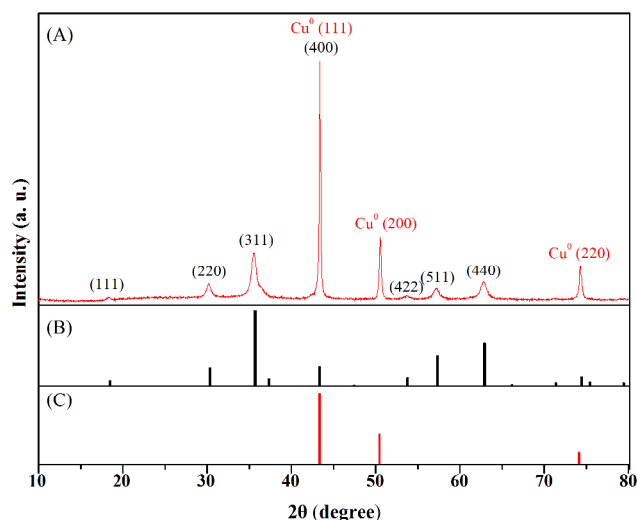


Fig. 3 (A) XRD pattern of CuFe_2O_4 MNCs; the standard diffraction lines of (B) CuFe_2O_4 (JCPDS card 77-0010) and (C) Cu (JCPDS card 85-1326).

The secondary structure of the MNCs was further confirmed by XRD measurements (Fig. 3). The positions and relative intensities of all diffraction peaks for resulting MNCs matched well with the data of standard CuFe_2O_4 (JCPDS card 77-0010) and copper (JCPDS card 85-1326). These peaks at $2\theta = 18.3, 30.2, 35.5, 43.3, 53.6, 57.1,$ and 62.7° are ascribed to (111), (220), (311), (400), (422), (511), and (440) reflections of cubic CuFe_2O_4 . Calculation with the Debye–Scherrer formula for the strongest peak (311) gave size of 14 nm for nanocrystals, which consisted with the HRTEM result. In addition, these peaks at $2\theta = 43.3, 50.4,$ and 74.1° are ascribed to (111), (200), and (220) reflections of fcc Cu crystal. Because ethylene glycol is a strong reducing agent under high temperature²⁸ and the reduction potential of Cu^{2+}/Cu is low (+0.34 V), the reduction of Cu^{2+} ions to Cu in the solvothermal system are possible. The presence of Cu in the solvothermal synthesis of CuFe_2O_4 particles has also been reported.^{29,30,23}

The magnetic property of MNCs was studied using a VSM at room temperature (Fig. 4). The saturation magnetization (M_s) value of CuFe_2O_4 MNCs was 45.1 emu g^{-1} , which was sufficient to accomplish fast and efficient separation with an external magnetic field. Furthermore, no remanence remained when the applied magnetic field was removed. The superparamagnetic property of the MNCs is critical for their applications in bioseparations, which prevent aggregation and enable them to redisperse rapidly when the magnetic field is removed. Notably, FT-IR spectrum of MNCs (Fig. S2†) indicated the existence of the citrate groups, which could greatly improve the water dispersibility and anti-aggregation properties of MNCs.³¹ As the inset of Fig. 4 shown, the well-dispersed MNCs in aqueous solution can be quickly attracted to the wall of the vial with the help of external magnet, and be redispersed quickly once the magnet was removed.

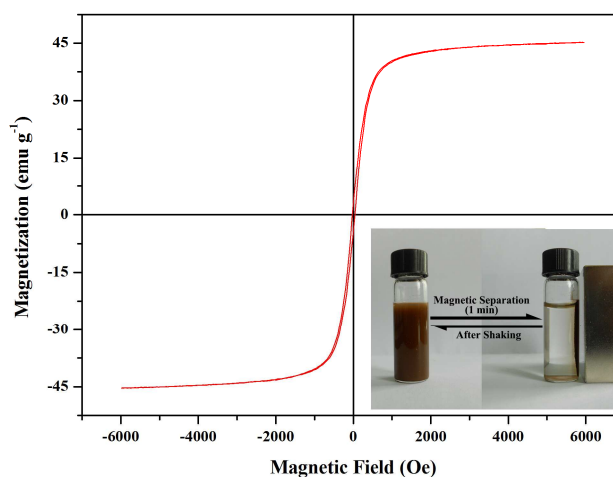


Fig. 4 Hysteresis loops of CuFe_2O_4 MNCs at 300K. The inset shows the magnetic separation behavior of CuFe_2O_4 MNCs.

To evaluate the surface area and porosity of the CuFe_2O_4 MNCs, the nitrogen adsorption-desorption isotherms at 77 K were measured (Fig. S3†). A typical type IV gas sorption isotherms was obtained, indicating the presence of mesopores. The BET surface area and total pore volume of CuFe_2O_4 MNCs were calculated to be $27.8 \text{ m}^2 \text{ g}^{-1}$ and $0.095 \text{ cm}^3 \text{ g}^{-1}$, respectively. The average pore size and were found to be 13.7 nm.

Binding properties of CuFe_2O_4 MNCs

Effect of pH on protein adsorption amounts. To explore the adsorption performances influenced by pH, a series of adsorption experiments with single component protein (BHb, BSA, HSA, Mb, Cyt C, Lyz and HRP) under different pH solution were investigated. As shown in Fig. 5, the maximum adsorption capacity for BHb was achieved at pH 7.0, which is close to the pI of BHb (6.8). When the pH was increased or decreased, the adsorption capacities for BHb were decreased rapidly, but still much higher than those of other proteins. In the cases of BSA (pI 4.7), HSA (pI 4.7), Mb (pI 7.3), Cyt C (pI 10.6) and Lyz (pI 11.4), the maximum adsorption capacities do not correlate with the pI values of these proteins (Fig. S4†). Therefore, the adsorption behaviors of these proteins cannot be simply explained by the electrostatic interactions. It is known that protein with an accessible electron-donor group (i.e. histidine, cysteine, and tryptophan) can bind to an IMAC surface.³² Among these electron donors, histidine is the primary amino acid binding with metal ions at neutral pH.³³ BHb is a His-rich protein containing 20 surface-exposed His residues³⁴ and thus can achieve maximum adsorption capacity at pH 7. BSA and HSA contain several surface-exposed acidic amino acid residues, including glutamic acid and aspartic acid. The adsorption capacities of BSA and HSA increased with the decrease of pH, which may indicate that CuFe_2O_4 MNCs have some degree of affinity toward acidic amino acid residues at low pH. Mb, Cyt C and Lyz also possess some surface-exposed glutamic acid and aspartic acid, and exhibit similar trend as

BSA and HSA. HRP is known as a glycoprotein containing 18% carbohydrate, which probably hinder the strong peptide-metal oxide interaction. The adsorption amount of HRP is lower than other proteins, the maximum adsorption capacities of HRP (pI 5.7) was achieved at pH 6, which could be explained by electrostatic interactions.

Above all, the exact mechanism of these relations remains unclear. But it is certain that the selective separation of BHB from protein mixture can be achieved in a neutral buffer solution.

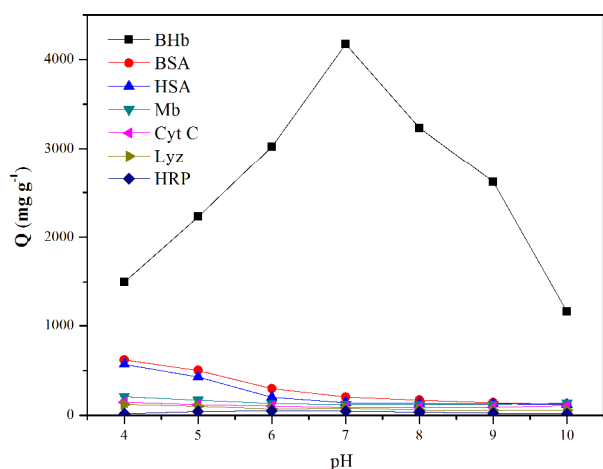


Fig. 5 pH dependence of the adsorption capacities of proteins (Bhb, BSA, HSA, Mb, Cyt C, Lyz and HRP) in phosphate buffer (pH 4.0-10.0) by CuFe_2O_4 MNCs.

Kinetic binding properties of CuFe_2O_4 MNCs. The adsorption kinetics of BHB onto CuFe_2O_4 MNCs at pH 7 was presented in Fig. 6A. It can be seen that the adsorption processes were time dependent and the CuFe_2O_4 MNCs displayed a fast adsorption rate. The adsorption capacity of BHB at a low concentrate of 0.10 mg mL^{-1} on CuFe_2O_4 MNCs increased rapidly in the first 3 min almost reached equilibrium after 5 min. Even in the case of a much higher initial concentration (1.0 mg mL^{-1}), the equilibrium was almost achieved within 10 min. The equilibrium time of the CuFe_2O_4 MNCs in this work was shorter than that of IMAC-based MNPs (Table 1). As shown in Fig. 6B and Table 2, the adsorption kinetics can be perfectly fitted by pseudo-second-order model ($R^2 > 0.999$), indicating that the chemical interactions were possibly involved in the sorption processes.³⁵ In addition, such fast initial adsorption rate ($>4456 \text{ mg g}^{-1} \text{ min}^{-1}$) and high adsorption capacity (4450 mg g^{-1}) could be ascribed to a higher density of copper (II) ions on the surface of CuFe_2O_4 MNCs than that of IMAC-based MNPs.⁹⁻¹³

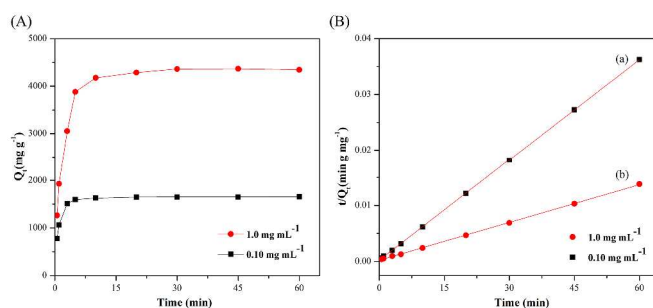


Fig. 6 (A) Adsorption kinetics of BHB (0.10 and 1.0 mg mL^{-1}) onto CuFe_2O_4 MNCs. (B) pseudo-second-order kinetics model to evaluate the kinetic mechanisms.

Table 1. Properties of different adsorbents for BHB capture

adsorbent	Capacity (mg g^{-1})	Size	Capture time
Cu-IDA-silica-coated Fe_3O_4 ⁹	418.6	350 nm	5 h
$\text{Fe}_3\text{O}_4@PVBC@IDA\text{-Ni}$ ¹³	1988	300 nm	1 h
$\text{Fe}_3\text{O}_4@SiO_2@IL$ ³⁶	2150	270 nm	15 min
CuFe_2O_4 MNCs (this work)	4175	170 nm	10 min

Table 2. A summary of the fitted parameters of the BHB adsorption kinetics on the CuFe_2O_4 MNCs.

Bhb	Pseudo-second-order kinetic model		
C_0 (mg mL^{-1})	Q_e (mg g^{-1})	V_0 ($\text{mg g}^{-1} \text{ min}^{-1}$)	R^2
0.10	1666	4597	0.9999
1.0	4450	4456	0.9997

Adsorption isotherms. To evaluate the selectivity and efficiency of the CuFe_2O_4 MNCs for His-exposed proteins, seven proteins with different number of exposure His residues were chosen as model proteins (Table 3). The adsorption capacity of these proteins with various initial concentrations ($0.10\text{--}1.0 \text{ mg mL}^{-1}$) in 20 mM PBS containing 0.2 M NaCl (pH = 7.0) is shown in Fig. 6. The saturated capacities had the following order: BHB \gg BSA $>$ HSA $>$ Mb $>$ Cyt C \approx Lyz $>$ HRP, respectively. In addition, the adsorption isotherms were fitted well to the Langmuir model (Table 3 and Fig. S5†).

In the His-mediated IMAC, the binding behaviours can be attributed principally to the following factors: (1) the number of accessible His residues, (2) the extent of a His residue's surface accessibility,³⁷ and (3) the microenvironment of the His residues, which refers to the amino acids within 15 \AA of a particular His residue.³⁸ MOAC is based on the same principle as IMAC, but MOAC materials don't have long-chain metal-chelating ligand as IMAC materials. Therefore, the steric hindrance effect in MOAC is more critical than that in IMAC. The water-accessibilities of the His residues were calculated by GETAREA 1.1 software³⁹ based on the protein crystal structure data from Protein Data Bank (PDB).⁴⁰ BHB (PDB code 2QSS) has as many as 20 water-accessible His residues, and 10 of them are accessible to CuFe_2O_4 MNCs. BSA (PDB code 3V03) has five water-accessible His residues (positions at 3, 59, 246, 378 and 509), but only two of them (His3 and His59) are accessible to CuFe_2O_4 MNCs. Therefore, the CuFe_2O_4 MNCs display a tremendous adsorption capacity for BHB and a rather lower capacity for BSA. Horse Mb (PDB ID: 1YMB) has six water-accessible His residues (positions at 36, 48, 81, 97, 113

and 116), and five of them (positions at 36, 48, 81, 113 and 116) may be responsible for the high affinity to IDA-Cu(II) columns.³⁷ However, only one His residues (His81) of Mb possesses suitable geography in the interaction with CuFe₂O₄ MNCs. Thus the adsorption amount of Mb is not as high as expected. HSA (PDB code 1AO6) has five (positions at 9, 128, 247, 367 and 510) water-accessible His residues, but none of them is accessible to CuFe₂O₄ MNCs. For horse Cyt C (PDB code 1HRC), Lyz (PDB code 1LYZ) and HRP (PDB code 1HCH), all histidines of them are little exposed (water-accessible surfaces <30%). Therefore, these proteins display relatively low affinity onto CuFe₂O₄ MNCs, and the adsorption mechanism of them should be different from that of BHB.

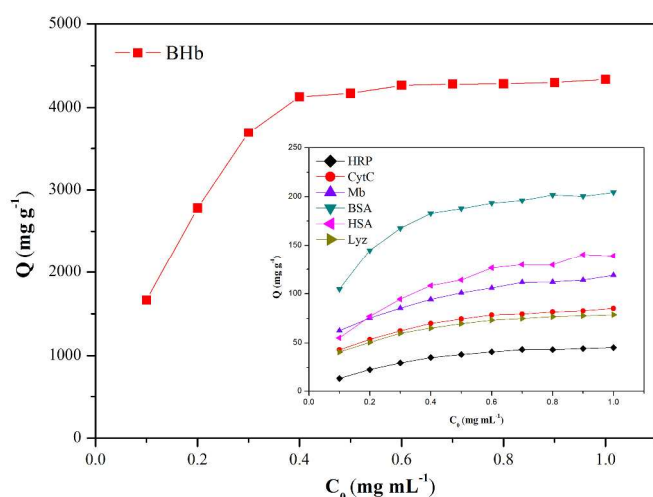


Fig. 7 Adsorption isotherms of proteins (BHB, BSA, HSA, Mb, Cyt C, Lyz and HRP) onto CuFe₂O₄ MNCs.

Table 3. A summary of the fitted parameters of the protein adsorption equilibrium on the CuFe₂O₄ MNCs.

protein	Mw (kDa)	pI	Langmuir model		
			Q _m (mg g ⁻¹)	b (L g ⁻¹)	R ²
BHB	64.5	6.8	4475	41.6	0.9995
BSA	66.7	4.7	213.2	20.0	0.9993
HSA	66.6	4.7	157.0	5.80	0.9945
Mb	17.7	7.3	129.0	9.53	0.9946
Cyt C	12.4	10.6	94.1	8.50	0.9976
Lyz	14.3	11.4	83.1	17.6	0.9963
HRP	44	5.7	56.5	4.63	0.9975

Quantitative assay of mixed adsorption using HPLC.

A more stringent test of the specificity of the CuFe₂O₄ MNCs for BHB is to immerse it in a protein mixture of BSA and BHB with a mass ratio of 1:3. Fig. 8a showed the HPLC chromatogram of unreacted protein mixture. After treating with CuFe₂O₄ MNCs, 93.4% BHB was removed from the mixture with minor loss of BSA (84.2% remained) (Fig. 8b). The result showed that CuFe₂O₄ MNCs could be used to remove high abundance BHB from mixture. As a negative control group, equal amount of Fe₃O₄ MNCs were used to treat the same mixture (Fig. 8c). The Fe₃O₄ MNCs showed little adsorption capacity and specificity for BHB (98.9% BSA and 97.4% BHB

remained). The different absorption behaviors between CuFe₂O₄ and Fe₃O₄ MNCs should be ascribed to the abundant surface Cu(II) sites of CuFe₂O₄ MNCs.

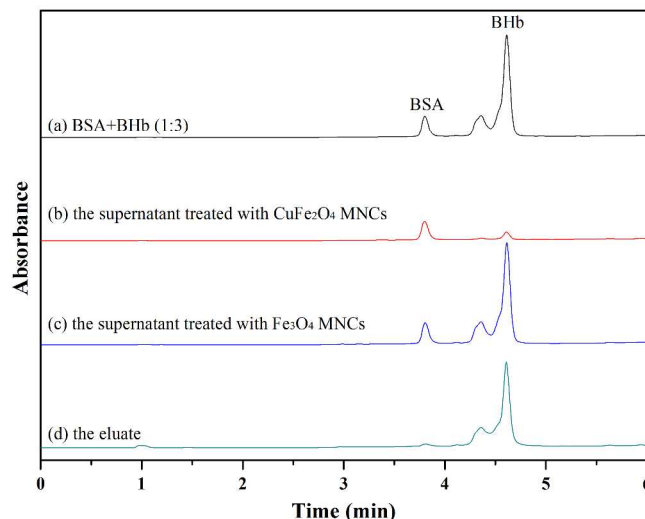


Fig. 8 HPLC chromatograms of unreacted protein mixture of 0.4 mg mL⁻¹ BSA and 1.2 mg mL⁻¹ BHB (a), the supernatant treated with CuFe₂O₄ MNCs (b) and Fe₃O₄ MNCs (c), and the eluate from CuFe₂O₄ MNCs–proteins conjugates (d).

Desorption is another important property for adsorbents. The captured BHB on the CuFe₂O₄ MNCs could be released by the treatment of the MNCs with histidine solution. As shown in Fig. 8d, 85.6% BHB were recovered by CuFe₂O₄ MNCs in the eluent.

The reusability of CuFe₂O₄ MNCs was tested. As shown in the Fig. S6, there is about 25% loss observed for the binding capacity of CuFe₂O₄ MNCs to BHB after the adsorption-regeneration cycle was repeated five times.

Application

The human blood sample was used to further evaluate the practicability and separation effectiveness of the CuFe₂O₄ MNCs in a real biological sample. The high-abundance hemoglobin in biological fluid is generally regarded as a drawback, since it seriously hindered the detection of low abundant proteins that are often marker of diseases. As described in the experimental section, human whole blood was diluted 100-fold and then incubated with CuFe₂O₄ and Fe₃O₄ MNCs. HHB is known to have 24 accessible His residues.³⁷ It is reasonable to expect that the CuFe₂O₄ MNCs will show high adsorption affinity for HHB.

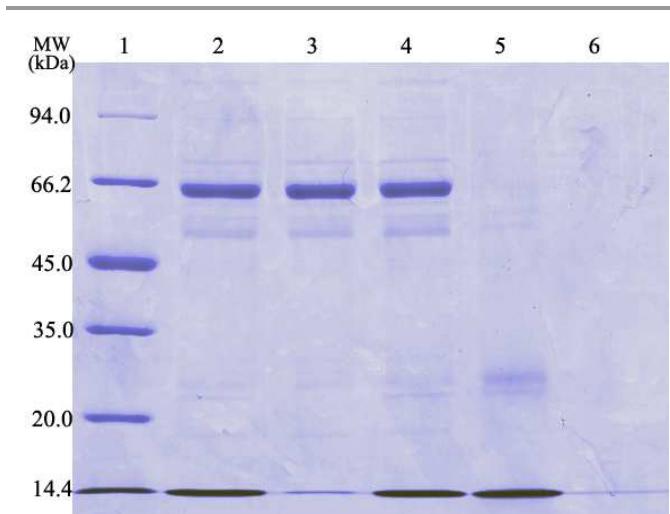


Fig. 9 SDS-PAGE analysis of human whole blood before and after treatment with CuFe_2O_4 and Fe_3O_4 MNCs. Lane 1, marker; lane 2, 100-fold human whole blood; lane 3, the supernatant after treatment with CuFe_2O_4 MNCs; lane 4, the supernatant after treatment with Fe_3O_4 MNCs; lane 5, the eluate from lane 3; lane 6, the eluate from lane 4.

As presented in Fig. 9, the separation of human whole blood without treatment (lane 2) revealed several major bands, which were mainly attributed to HSA and HHb proteins. Lane 3 showed the supernatant after treatment with CuFe_2O_4 MNCs, in which less than 3% HHb (quantification of the protein bands was performed with Quantity One software (Bio-Rad)) was left. Namely, nearly 97% HHb was captured by CuFe_2O_4 MNCs, but the other proteins including HSA (95% remained) were almost reserved. Moreover, the band of HHb reappeared in the eluent of CuFe_2O_4 MNCs-proteins conjugates (lane 5), and the recovery of HHb reached 90%. Compared with CuFe_2O_4 MNCs, all proteins including HHb still existed in the supernatant after treatment with Fe_3O_4 MNCs (lane 4), and none of protein bands were found in the eluent (lane 6), demonstrating the lack of availability of Fe_3O_4 MNCs. Overall, the SDS-PAGE analysis confirmed the practicability of CuFe_2O_4 MNCs for the selective depletion of high-abundance hemoglobin in blood samples.

Conclusions

In the study, we reported a facile ligand-free method for the rapid and highly specific separation of His-rich proteins by using CuFe_2O_4 magnetic nanocrystal clusters (MNCs). Monodisperse CuFe_2O_4 MNCs were synthesized *via* a simple and economical one-pot hydrothermal process. The measurements indicated that the MNCs exhibited good dispersion, high crystallinity, high saturation magnetization (45.1 emu g^{-1}) and superparamagnetic properties. The CuFe_2O_4 MNCs exhibit high haemoglobin binding capacity (4475 mg g^{-1}) owing to the coordination between Copper (II) ions and surface-exposed His residues of haemoglobin. In addition, the CuFe_2O_4 MNCs were successfully employed to selectively bind and removal abundant protein haemoglobin from human blood

samples. The good results demonstrated their potential in separation of His-rich proteins from biological samples.

Acknowledgements

This study was supported by the National Natural Science Foundation of China (21375018 and 21275029), National Science Foundation for Fostering Talents in Basic Research of China (No. J1103303), the National Natural Science Funds for Distinguished Young Scholar (21125524), the Natural Science Foundation of Fujian Province (2014J01402), and the Program for Changjiang Scholars and Innovative Research Team in University (No. IRT1116).

Notes and references

^a Ministry of Education Key Laboratory of Analysis and Detection for Food Safety, Fujian Provincial Key Laboratory of Analysis and Detection Technology for Food Safety, College of Chemistry, Fuzhou University, Fuzhou, Fujian, 350002, China.

E-mail: zianlin@fzu.edu.cn (Z.A. Lin); zlan@fzu.edu.cn (L.Zhang); Fax: +86-591-22866135

† Electronic Supplementary Information (ESI) available. See DOI: 10.1039/b000000x/

1. M. Rowinska-Zyrek, D. Witkowska, S. Potocki, M. Remelli, and H. Kozlowski, *New J. Chem.*, 2013, **37**, 58–70.
2. M. de Souza Castilho, T. Laube, H. Yamanaka, S. Alegret, and M. I. Pividori, *Anal. Chem.*, 2011, **83**, 5570–5577.
3. Y. Li, X. M. Zhang, and C. H. Deng, *Chem. Soc. Rev.*, 2013, **42**, 8517–8539.
4. Y. Pan, X. Du, F. Zhao, and B. Xu, *Chem. Soc. Rev.*, 2012, **41**, 2912–2942.
5. C. J. Xu, K. M. Xu, H. W. Gu, X. F. Zhong, Z. H. Guo, R. K. Zheng, X. X. Zhang, and B. Xu, *J. Am. Chem. Soc.*, 2004, **126**, 3392–3393.
6. C. J. Xu, K. M. Xu, H. W. Gu, R. K. Zheng, H. Liu, X. X. Zhang, Z. H. Guo, and B. Xu, *J. Am. Chem. Soc.*, 2004, **126**, 9938–9939.
7. E. J. Cho, S. Jung, K. Lee, H. J. Lee, K. C. Nam, and H.-J. Bae, *Chem. Commun.*, 2010, **46**, 6557–6559.
8. H. Y. Xie, R. Zhen, B. Wang, Y. J. Feng, P. Chen, and J. Hao, *J. Phys. Chem. C*, 2010, **114**, 4825–4830.
9. M. Zhang, D. Cheng, X. W. He, L. X. Chen, and Y. K. Zhang, *Chem. Asian J.*, 2010, **5**, 1332–1340.
10. M. Zhang, X. W. He, L. X. Chen, and Y. K. Zhang, *J. Mater. Chem.*, 2010, **20**, 10696–10704.
11. M. Zhang, X. W. He, L. X. Chen, and Y. K. Zhang, *Nanotechnology*, 2011, **22**, 065705.
12. G. Q. Jian, Y. X. Liu, X. W. He, L. X. Chen, and Y. K. Zhang, *Nanoscale*, 2012, **4**, 6336–6342.
13. J. L. Cao, X. H. Zhang, X. W. He, L. X. Chen, and Y. K. Zhang, *J. Mater. Chem. B*, 2013, **1**, 3625–3632.
14. I. S. Lee, N. Lee, J. Park, B. H. Kim, Y.-W. Yi, T. Kim, T. K. Kim, I. H. Lee, S. R. Paik, and T. Hyeon, *J. Am. Chem. Soc.*, 2006, **128**, 10658–10659.
15. S.-Y. Huang and Y.-C. Chen, *Anal. Chem.*, 2013, **85**, 3347–3354.

16. M. F. Shao, F. Y. Ning, J. W. Zhao, M. Wei, D. G. Evans, and X. Duan, *J. Am. Chem. Soc.*, 2011, **134**, 1071–1077.
17. Z. Liu, M. Li, F. Pu, J. S. Ren, X. J. Yang, and X. G. Qu, *J. Mater. Chem.*, 2012, **22**, 2935–2942.
18. J. Chun, S. W. Seo, G. Y. Jung, and J. Lee, *J. Mater. Chem.*, 2011, **21**, 6713–6717.
19. Z. Liu, M. Li, X. J. Yang, M. L. Yin, J. S. Ren, and X. G. Qu, *Biomaterials*, 2011, **32**, 4683–4690.
20. J. Lee, S. Y. Lee, S. H. Park, H. S. Lee, J. H. Lee, B.-Y. Jeong, S.-E. Park, and J. H. Chang, *J. Mater. Chem. B*, 2013, **1**, 610–616.
21. J. X. Zhao, Y. L. Cheng, X. B. Yan, D. F. Sun, F. L. Zhu, and Q. J. Xue, *CrystEngComm*, 2012, **14**, 5879–5885.
22. R. Z. Zhang, J. M. Liu, S. F. Wang, J. Z. Niu, C. G. Xia, and W. Sun, *ChemCatChem*, 2011, **3**, 146–149.
23. M. Y. Zhu, D. H. Meng, C. J. Wang, and G. W. Diao, *ACS Appl. Mater. Interfaces*, 2013, **5**, 6030–6037.
24. Z. A. Lin, J. N. Zheng, F. Lin, L. Zhang, Z. W. Cai, and G. N. Chen, *J. Mater. Chem.*, 2011, **21**, 518–524.
25. Z. A. Lin, J. N. Zheng, Z. W. Xia, H. H. Yang, L. Zhang, and G. N. Chen, *RSC Adv.*, 2012, **2**, 5062–5065.
26. S. Libert, V. Gorshkov, D. Goia, E. Matijević, and V. Privman, *Langmuir*, 2003, **19**, 10679–10683.
27. J. P. Ge, Y. X. Hu, M. Biasini, W. P. Beyermann, and Y. D. Yin, *Angew. Chem. Int. Ed.*, 2007, **46**, 4342–4345.
28. H. Deng, X. L. Li, Q. Peng, X. Wang, J. P. Chen, and Y. D. Li, *Angew. Chemie Int. Ed.*, 2005, **44**, 2782–2785.
29. N. Bao, L. Shen, Y. Wang, P. Padhan, and A. Gupta, *J. Am. Chem. Soc.*, 2007, **129**, 12374–12375.
30. E. Solano, L. Perez-Mirabet, F. Martinez-Julian, R. Guzmán, J. Arbiol, T. Puig, X. Obradors, R. Yañez, A. Pomar, S. Ricart, and J. Ros, *J. Nanopart. Res.*, 2012, **14**, 1034.
31. J. Liu, Z. K. Sun, Y. H. Deng, Y. Zou, C. Y. Li, X. H. Guo, L. Q. Xiong, Y. Gao, F. Y. Li, and D. Y. Zhao, *Angew. Chem. Int. Ed.*, 2009, **48**, 5875–5879.
32. R. J. Todd, R. D. Johnson, and F. H. Arnold, *J. Chromatogr. A*, 1994, **662**, 13–26.
33. R. S. Tirumalai, K. C. Chan, D. A. Prieto, H. J. Issaq, T. P. Conrads, and T. D. Veenstra, *Mol. Cell. Proteomics*, 2003, **2**, 1096–1103.
34. G. E. Wuenschell, E. Naranjo, and F. H. Arnold, *Bioprocess Eng.*, 1990, **5**, 199–202.
35. C. M. Dai, J. Zhang, Y. L. Zhang, X. F. Zhou, Y. P. Duan, and S. G. Liu, *Chem. Eng. J.*, 2012, **211–212**, 302–309.
36. Y. Wei, Y. Li, A. Tian, Y. Fan, and X. Wang, *J. Mater. Chem. B*, 2013, **1**, 2066–2071.
37. E. S. Hemdan, Y. J. Zhao, E. Sulkowski, and J. Porath, *Proc. Natl. Acad. Sci.*, 1989, **86**, 1811–1815.
38. A. J. Russell and A. R. Fersht, *Nature*, 1987, **328**, 496–500.
39. R. Fraczekiewicz and W. Braun, *J. Comput. Chem.*, 1998, **19**, 319–333.
40. H. M. Berman, J. Westbrook, Z. Feng, G. Gilliland, T. N. Bhat, H. Weissig, I. N. Shindyalov, and P. E. Bourne, *Nucleic Acids Res.*, 2000, **28**, 235–242.

Graphical abstract

A facile one-pot method was developed for synthesis of CuFe_2O_4 magnetic nanocrystal clusters and its application in ligand-free separation of histidine-rich proteins.

